Transformation behavior and inverse caloric effects in magnetic shape memory $Ni_{44-x}Cu_xCo_6Mn_{39}Sn_{11}$ ribbons

A. Wójcik[a], C. Aguilar-Ortiz[b], W. Maziarz[a], M.J. Szczerba[a], M. Sikora[c], A. Żywczak[c], P.Álvarez-Alonso[d], E. Villa[e], H. Flores-Zúñiga[b], E. Cesari[f], V.A. Chernenko[d, g]

[a]Institute of Metallurgy and Materials Science, Polish Academy of Sciences, 25 Reymonta Street, 30-059 Kraków, Poland

[b]Potosino de Investigación Científica y Tecnológica A.C., San Luis Potosí 78216, Mexico

[c]Academic Centre on Materials and Nanotechnology, AGH University of Science and Technology, Al. Mickiewicza 30, 30-059 Kraków, Poland

[d]BCMaterials & University of Basque Country (UPV/EHU), 48080 Bilbao, Spain

[e]CNR IENI Unità di Lecco, 23900 Lecco, Italy

[f]Departament de Física, Universitat de les Illes Balears, Ctra. De Valldemossa, km 7.5, E-07122 Palma de Mallorca, Spain

[g]Ikerbasque, Basque Foundation for Science, 48013 Bilbao, Spain

Abstract

An influence of the Cu doping on the structural, magnetic and thermoelastic properties of the Heusler $Ni_{44-x}Cu_xCo_6Mn_{39}Sn_{11}$ (x=1–4 at.%) ribbons has been investigated. It is found that the addition of Cu stabilizes austenite phase. Martensite transformation (MT) temperatures generally decrease when Cu concentration increases, which is atributed to the atom size effect. The inverse magnetocaloric and elastocaloric effects in the vicinity of MT under moderate magnetic fields and stresses have been evaluated. Small Cu addition enhances both effects as compared to quaternary Ni–Co–Mn–Sn alloy.

1. Introduction

Many studies have been performed on Ni–Co–Mn–Sn metamagnetic shape memory alloys (MMSMAs) (see, e.g., Refs.[1-3]). These materials undergo a first order martensitic

transformation (MT) from ferromagnetic austenite to weak magnetic martensite. Due to a large magnetization difference (ΔM) between the high temperature parent phase-austenite and low-temperature martensite phase a field induced reverse martensitic transformation (FIRMT) occurs. This phenomenon results in a metamagnetic shape memory effect (MMSME) and an inverse magnetocaloric effect (IMCE). For IMCE, a positive magnetic entropy change ($\Delta S_M \geq 0$) and a negative adiabatic temperature change ($\Delta T_{ad} \leq 0$) is observed, which means that the sample cools down when magnetic field is adiabatically applied (in contrast to the conventional MCE) [4].

From practical point of view, a good magnetocaloric material should be characterized by the MT temperature near room temperature and should exhibit appropriate magnetocaloric properties, i.e. high values of the magnetic entropy change, ΔS_M, as well as the refrigerant capacity (RC) at low magnetic fields [5]. Cong et al. have studied the influence of Co addition on magnetic properties and phase transformation temperature in $Ni_{50-x}Co_xMn_{39}Sn_{11}$ alloys. It is found that $Ni_{44}Co_6Mn_{39}Sn_{11}$ bulk alloy exhibits the largest ΔM across MT. However, the MT temperature is quite high for such an alloy equal to about 342 K [6]. On the other hand, it is known that the MT temperature and magneto-structural properties of Ni–Mn based Heusler alloys are very sensitive to a chemical composition and multiple doping. We assume that, particularly, an addition of Cu into the aforementioned $Ni_{44}Co_6Mn_{39}Sn_{11}$ alloy could be effective tool to fine control the temperature range of MT and improve its magneto-structural properties, as it is known that Cu substitution for Ni and Mn in the ternary Ni–Mn–Sn and Ni–Mn–Ga alloys could effectively tailor the magneto-structural transformation by affecting the magnetic coupling between Mn atoms [7]. As an example, the addition of 2 at.% of Cu into $Ni_{46}Mn_{43}Sn_{11}$ decreases both the MT and Curie temperature of austenite (T_C^A) while increases the value of ΔM resulting in an increase of ΔS_M [7]. Huu et al. have also reported a decrease of the MT temperature with Cu addition in $Ni_{50-x}Cu_xMn_{37}Sn_{13}$ (x=0, 1, 2, 4, 8 at.%)

alloys exhibiting relatively large values of ΔS_M (5.4 J $kg^{-1}K^{-1}$ at 15 kOe) [8]. In the case of $Ni_{50-x}Cu_xMn_{36}Sn_{11}$ (x=2, 4, 6 at.%) alloys, the T_C^A temperature slightly increases, while the MT temperature decreases upon Cu addition [9]. Note, that the decrease of MT temperature as a function of Cu doping is opposite to what it is expected from the increase of valence electron concentration (*e*/*a*) [10]. This decrease can be explained by the enlargement of the unit cell volume caused by replacing smaller atoms (Ni) by the larger ones (Cu) [11]. Furthermore, the addition of Cu into MMSMAs can enhance their ductility like in the case of Ni–Mn–Ga [12]. Castillo-Villa et al. have investigated the inverse magnetocaloric and conventional elastocaloric (eCE) effects in $Ni_{43}Mn_{40}Sn_{10}Cu_7$. Interestingly that IMCE was observed in latter alloy that shows a paramagnetic character of both austenite and martensite in a zero field. This fact reflects a strong coupling between the magnetic and crystal lattice degrees of freedom in MMSMAs [13].

An influence of fifth element on the magnetocaloric effect and magneto-structural properties of Ni–Co–Mn–Sn has been reported in Refs. [14-16]. The results show that manufacturing of quinary alloys allows a fine tuning of MT temperature and improving their physical properties.

Another factor affecting the transition temperatures and magneto-structural properties of MMSMAs is a fabrication method. Many reports concern just bulk alloys prepared by the arc- or induction melting methods. However, bulk alloys require a time consuming heat treatment in order to obtain a good homogeneity and desirable properties. On the other hand, melt-spinning process allows obtaining polycrystalline ribbons of good homogeneity leading to shortening of heat treatment time while enhancing MCE [17-19]. Furthermore, the ribbon shape is favorable for the applications [20].

This work presents the systematic study of the influence of Cu substitution for Ni on the structural, transition and magnetic characteristics exhibiting by the Heusler Ni_{44-}

$_xCu_xCo_6Mn_{39}Sn_{11}$ (x=1–4 at.%) ribbons. Furthermore, both inverse magnetocaloric as well as inverse elastocaloric effects have been investigated.

2. Experimental

A series of $Ni_{44-x}Cu_xCo_6Mn_{39}Sn_{11}$ alloys with x=0, 1, 2, 3, 4 at. %, hereafter referred to as Cu0, Cu1, Cu2, Cu3 and Cu4, respectively, were prepared by induction melting from the high purity (>99.99) elements in argon atmosphere. The extra 2 at. % of manganese was added to compensate losses connected with its evaporation during fabrication process. The as-cast ingots were subsequently annealed at 1223 K for 5h. under argon atmosphere in order to ensure a good homogeneity. Then, the ribbons were fabricated by melting and ejecting with 0.25 MPa overpressure onto a copper wheel rotating at the linear speed of 30 m s^{-1}.

The microstructure and chemical composition of ribbons were examined by using Philips XL30 Scanning Electron Microscope (SEM) and Tecnai G2 Transmission Electron Microscope (TEM) equipped with energy dispersive X-ray microanalyser (EDX). Thin foil samples for TEM observations were prepared with TenuPol-5 double jet electropolisher using an electrolyte of nitric acid (1/3) and methanol (2/3) at temperature of about 243 K. Room temperature X-ray diffraction (XRD) patterns were collected by a Bruker D8 diffractometer using a Co radiation. Lattice parameter of paramagnetic austenite was studied by a Bruker D8 at temperature of 430 K. Transformation behavior and thermal effects were investigated by a differential scanning calorimetry (DSC) using Metler DSC 823 instrument with cooling/heating rate of 10 K min^{-1}. Magnetic properties as well as the characteristic temperatures of martensitic and magnetic transitions were examined by the LakeShore 7407 vibrating sample magnetometer (VSM) equipped with a Janis made LN_2 cryostat. Temperatures of both martensitic and magnetic transitions were estimated from the temperature dependences of physical properties by the two-tangents method. The thermomechanical measurements were carried out with a stress-control option of operation in

a Q800 TA Instruments Mechanical Analyzer (DMA) using the dynamic mode (temperature rate of 2 K min^{-1}, strain amplitude of 10^{-4} and frequency of 1Hz) and static one (temperature dependence of strain $\varepsilon(T)$ were measured under load applied along the ribbons axis with temperature rate of 5 K min^{-1}). Isothermal stress-strain (σ-ε) curves were registered with a rate of 2.5 MPa min^{-1}.

3. Results and discussion

3.1 Microstructure and structure characterization

The microstructure and chemical composition of $Ni_{44-x}Cu_xCo_6Mn_{39}Sn_{11}$ (x=1, 2, 3, 4 at. %) melt-spun ribbons have been investigated by SEM and TEM microscopy. Figure 1 demonstrates SEM secondary electron (SEM SE) images of Cu1 ribbon taken at the free side. All ribbons possess a similar microstructure consisting of two types of grains, independently on the chemical composition. The first type is given by small equiaxed grains with the size of about 1–2 μm while the second type is represented by larger cells with various shapes being arranged in so-called clusters. Similar result was already observed in the $Ni_{48}Mn_{39.5}Sn_{12.5}$ ribbons by Czaja et al. [21]. It was also found that the free surface exhibits coarser morphology in comparison to the wheel side. Furthermore, one can see the difference in the microstructure between the initial alloy with the composition $Ni_{44}Co_6Mn_{39}Sn_{11}$ (referred to as Cu0), investigated in our previous work (Ref. [22]) and Cu-doped ribbons. It was shown that the microstructure of the quaternary alloy is composed of fine equiaxed grains, cells being more complicated in shapes and large grains of about 10–15 μm with martensite plates inside. The divergence between ribbons seems to be connected with the addition of the fifth element which affects the characteristic temperatures of MT as well as the crystal structure and microstructure.

The chemical compositions of $Ni_{44-x}Cu_xCo_6Mn_{39}Sn_{11}$ (x=1, 2, 3, 4 at. %) melt-spun ribbons were analyzed by the EDX method. The results taken from the free side are listed in

Table 1. Moreover, detailed investigation shows that there is no difference in the distribution of elements between the free and the wheel side surfaces of the ribbons as well as along their cross-section. This was also shown by Santos et al. in the case of $Ni_{50}Mn_{37}Sn_{13}$ ribbons [23]. Based on the EDX results the valence electron concentration per atom, *e*/*a*, was estimated as shown in the last column of Table 1. This was calculated from the sum of *d* and *s* electrons for Mn (7), Ni (10), Co (9), Cu (11), and *s* and *p* electrons for Sn (4). Table 1 shows that the substitution of Cu for Ni leads *e*/*a* to increase with respect to the initial alloy (*e*/*a*=8.15).

Figure 2 presents TEM bright field (BF) images captured from the grain interior (a) and grain boundary (c) of Cu1 ribbon at room temperature. The corresponding selected area electron diffraction patterns (SAEDPs) are indexed in terms of the cubic $L2_1$ structure with [100] zone axis (b) and six-layered 12M martensite with [210] zone axis (d). Five additional spots between two fundamental maxima are easily obseved. This type of martensite is not often observed in MMSMAs, contrary to four-, five- and seven-layered structures. However, it has been found in the alloys, such as $Ni_{44}Co_6Mn_{39}Sn_{11}$ [22], $Ni_{50}Mn_{40}Sn_{10}$ [24], and $Ni_{44.5}Co_{5.5}Mn_{39.5}Sn_{10.5}$ after homogenization for long time [25]. Moreover, it is clearly seen that martensite plates evolve from the grain boundaries of austenitic grains. This may be connected with two reasons such as grain boundaries represent favored places for the nucleation and the microsegregation of elements between grain boundaries and grain interiors afecting the *e*/*a* value. The coexistance of austenite and martensite as a consequence of local compositional fluctuation has been reported in the case of $Ni_{46}Mn_{41.5-x}Fe_xSn_{12.5}$ [26] and $Ni_{50-x}Mn_{37.5+x}Sn_{12.5}$ [27]. Cu2 also reveals mixed microstructure consisting of austenite and martensite. Figure 3 shows BF images and corresponding SAEDPs for Cu3. Besides $L2_1$ austenite small amount of martensite phase, being indexed as the 4O orthorhombic four-layered structure, is also visible. Cu4 ribbon is found to be in a single austenite form. Thus, one can conclude that at room temperature the crystal structure of the investigated ribbons

evolves in the following sequence: 12M+$L2_1$ (Cu0) → $L2_1$+12M (Cu1, Cu2) → $L2_1$+4O (Cu3) → $L2_1$ (Cu4). It is obvious the substitution of Ni by Cu results in the stabilization of austenite.

XRD measurements confirm TEM observations. Figure 4 depicts X-ray diffraction patterns of $Ni_{44-x}Cu_xCo_6Mn_{39}Sn_{11}$ (x=1–4 at.%) ribbons at room temperature taken from the free side. It is found that Cu1 and Cu2 ribbons reveal the mixture of $L2_1$ structure with trace amount of martensite being identified as a 12M six-layered martensite. Ribbons containing 3 and 4 at.% of Cu have pure $L2_1$ austenitic structure. No extra peaks indicating an existence of the additional phases are observed. In the case of Cu3, martensite phase is not detected by X-ray diffraction patterns. This might be connected with a small amout of martensite which is below detection limit of XRD.

Furthermore, the lattice parameter a_c and unit cell volume V_c of $L2_1$ paramagnetic austenite for all ribbons were estimated and plotted in Figure 5. Calculations were made based on X-ray measurements carried out at 430 K in order to obtain fully austenite phase. It is seen that the lattice parameters as well as the unit cell volume rise up with the increase of the concentration of Cu in $Ni_{44-x}Cu_xCo_6Mn_{39}Sn_{11}$ ribbons. It is attributed to the substitution of smaller Ni atoms with the atomic radius of 0.125 nm by larger Cu atoms with the atomic radius of 0.128 nm [28].

3.2 Transformation behavior and magnetic characterisation

Figure 6 depicts DSC cooling and heating curves for $Ni_{44-x}Cu_xCo_6Mn_{39}Sn_{11}$ (x=0, 1, 2, 3 at .%) melt spun ribbons. One can see exothermic and endothermic peaks corresponding to the forward and reverse martensitic transformation with start and finish characteristic temperatures (T_{ms}, T_{mf}, T_{as}, T_{af}), respectively. The transformation temperatures T_M and T_A are determined as (T_{ms}+T_{mf})/2 and (T_{as}+T_{af})/2, respectively. The width of thermal hysteresis, being a consequence of the first-order nature of MT, was calculated as a difference between

austenite finish and martensite start temperatures (ΔT=T_{af}-T_{ms}). DSC curves enable also an estimation of the averaged MT enthalpy change ($|\Delta H|$), calculated as the area under the exothermic and endothermic peaks. The entropy change of MT (ΔS) was estimated as $|\Delta H|/T_0$, where T_0 is (T_{ms}+T_{af})/2. All results are listed in Table 2. Note that the DSC curves for Cu4 are not shown here, because MT takes place below the studied temperature range.

The thermomagnetization dependences, $M(T)$, for all ribbons are shown in Figure 7. They were measured under external magnetic field of 200 Oe during cooling (FC) and heating (FH). Upon cooling, samples undergo the magnetic transition from paramagnetic austenite to ferromagnetic austenite. During further cooling, the martensitic transformation from austenite to martensite with characteristic hysteresis is observed. The values of the characteristic MT temperatures (see Table 2) are in good agreement with data of the calorimetric measurements. Small variations between results are ascribed to the influence of different cooling/heating rates.

It is well-known that the MT temperatures in the Heusler type SMAs are controlled by two main factors: (i) electron valence concentration and (ii) unit-cell volume [10, 29]. In the case of studied $Ni_{44-x}Cu_xCo_6Mn_{39}Sn_{11}$ (x=0–4 at.%) alloys, the MT temperatures are drastically shifted to lower temperatures with the addition of 1 at. % of Cu. Then, slightly increase for Cu2 ribbon. Further addition of Cu leads again to their decrease. Such a complex behavior was observed in $Ni_{50}Mn_{40-x}Sn_{10}Fe_x$ as a result of the precipitation of the additional phases [30]. However, in the studied alloys no obvious signs of the precipitates were found. The aforementioned irregular behavior may be attributed to the *e*/*a* decrease from 8.15 to 8.13, with regard to Cu0 [22], and further increase up to 8.16. Nevertheless, the general tendency for the MT temperatures in the studied ribbons is their decrease with increasing of the Cu concentration being opposite to the *e*/*a* rule. Figure 5 shows that the difference in atomic radius can be responsible for the reduction of the MT temperatures. As already

mentioned, the atomic radius of Cu and Ni is 0.128 and 0.125 nm, respectively [28]. Thus, replacing smaller Ni atoms by larger Cu atoms results in the decrease of the MT temperature. Many reports concerning Cu-doped Ni-Mn based Heusler alloys show similar results pointing out that the unit cell volume factor prevails over *e*/*a* [7–9, 31]. It is worth noting that the concept of the hybridization between Ni 3d and Mn 3d states was also put forward as an additional factor [32]. Accordingly, any change in Mn and Ni content as well as Cu addition may lead to the weakening the hybridization resulting in a reduction of the MT temperatures. This behavior has been observed in $Mn_{50}Ni_{40-x}Cu_xSn_{10}$ [33], $Ni_{50}Mn_{36-x}Co_xSn_{14}$ [34], $Ni_{50+x}Mn_{37-x}Sb_{13}$ and $Ni_{50}Mn_{37+x}Cr_xSb_{13}$ [35].

Magnetic and DSC measurements, as well as data from Table 2, show that T_c^A also shifts to lower temperatures with the replacement of Ni by Cu, which correlates with the increase of the volume cell of austenite. This is in line with fact that the hydrostatic pressure increases the Curie temperature of austenite [36]. Aguilar-Ortiz et al. confirmed that the substitution of smaller Ni atoms by larger Fe atoms leads to the enlargement of the austenite volume cell which causes T_c^A to decrease [37].

Figure 8 shows the magnetization curves, $M(H)$, at different temperatures around the martensitic transformation. The measurements were performed up to 15 kOe after every time zero-field cooling to temperature below T_{mf} in order to achieve fully martensite structure. Samples show metamagnetic behavior in temperature range of 248–299K, 242–302K, 216–288K, 165–210K for Cu1, Cu2, Cu3, Cu4, respectively. The magnetic hysteresis corresponds to the magnetic field induced reversible martensitic transformation from martensite to austenite and back to martensite.

3.2 Inverse magnetocaloric and elastocaloric effects

Magnetic entropy change (ΔS_M) has been estimated from magnetic isotherms using Maxwell's relation $\Delta S_M(T,H) = \int_0^H \left(\frac{\partial M}{\partial T}\right)_H dH$, where M and H are magnetization and

magnetic field, respectively. Temperature dependences of ΔS_M under magnetic field of 15 kOe are shown in Figure 9. Peak value of ΔS_M for Cu0, Cu1, Cu2, Cu3 alloys is 2.9 J kg^{-1}K^{-1} (345K), 2.1 J kg^{-1}K^{-1} (275K), 6.3 J kg^{-1}K^{-1} (293K) and 4.3 J kg^{-1}K^{-1} (258K), respectively. The result for Cu4 ribbon is not shown here, due to its negligible value. It is known that total entropy change during MT (ΔS^{MT}) contains the vibrational and magnetic contributions. Furthermore, the ΔS^{MT} is highly dependent on the difference between Curie of austenite and martensitic transformation temperatures (T_c^A-T_M). With the increase of the value of (T_c^A-T_M), ΔS^{MT} drops exponentially because of the magnetic contribution reduction [38]. In the case of Cu4 the difference between Curie point of austenite and martensite temperature is close to 200 K, which results in extremely low value of ΔS_M. From the practical viewpoint, refrigerant capacity (RC) is important parameter, which describes the total amount of thermal energy that can be transferred between hot and cold sinks in one ideal thermodynamic cycle. RC has been calculated by using the following equation: RC=$\left|\Delta S_M^{peak}\right| \times \delta T_{FWHM}$, where ΔS_M^{peak} is the maximum at ΔS_M(T) curve and δT_{FWHM} is the full-width at half maximum of the same curve obtained under magnetic field change of 15 kOe. Furthermore, due to the first order nature of MT, the average hysteresis loss (HL) was calculated by the estimation of the area of $M(T)$ curves at different temperatures. The effective RC_{eff} has been obtained by subtracting HL from the total RC [39-41]. The quantified values of RC_{eff} in magnetic field of 15 kOe for Cu0, Cu1, Cu2, Cu3 ribbons are 19 J kg^{-1}, 31.4 J kg^{-1}, 41.9 J kg^{-1}, 50.8 J kg^{-1}, respectively. One can see that, the addition of 2 at. % of Cu increases the value of ΔS_M for more than two times in the magnetic field of 15 kOe. Moreover Cu addition leads to the enhancement of RC_{eff} (Cu2, Cu3), while tuning the MT temperature close to ambient temperature.

Figure 10 (a,b) depicts temperature dependences of strain, $\varepsilon(T)$, recorded under various applied tensile stresses for $Ni_{44}Co_6Mn_{39}Sn_{11}$ and $Ni_{42}Cu_2Co_6Mn_{39}Sn_{11}$ ribbons. The application of the stress higher than 20-30 MPa causes ribbons to fail due to their high

brittleness. The measurements were performed only for two ribbons due to limitation connected with the required geometry of ribbons such as length and width. Temperatures of reverse martensitic transformations (T_A) were estimated from ε(T) curves and plotted in Figure 10(c) for both ribbons. T_A temperature is shifted to lower temperatures with the increase of external stresses compared to the temperatures measured under 1MPa, which gives rise to stress-induced reverse martensitic transformation. This phenomenon has been observed previously on the $Ni_{50}Mn_{40}Sn_{10}$ ribbon [42] being associated with the internal compressive stress introduced during fabrication process. This compressive stress opposes the external tensile stress. The isothermal entropy change (ΔS) was calculated by means of Maxwell's relationship: $\Delta S(T,\sigma) = \int_0^\sigma \left(\frac{\partial \varepsilon}{\partial T}\right)_\sigma d\sigma$, where σ and ε are uniaxial stress and corresponding strain, respectively. Results for Cu0 and Cu2 ribbons are shown in Figure 11. The maxima in ΔS versus T under the stress of about 30 MPa correspond to about 0.2 J $kg^{-1}K^{-1}$ for Cu0 and 0.5 J $kg^{-1}K^{-1}$ for Cu2 ribbon. Both values of ΔS are above zero indicating the inverse elastocaloric effect (see Ref.[42]). This effect is associated with the anomalous stress-induced reverse MT that occurs in both ribbons and can be considered as an analog of the inverse magnetocaloric effect in Ni–Mn–Ga Heusler alloys [42]. Additionally, the inverse elastocaloric effect has been also found in Fe-Rh [43] and in the decomposed Ti-Ni [44] alloys. In both cases, it was attributed to the stress-induced structural transformation due to the volume contraction across the structural transformation and internal stress caused by precipitates, respectively.

4. Conclusions

In summary, we have systematically studied the influence of the substitution of Ni by Cu in $Ni_{44-x}Cu_xCo_6Mn_{39}Sn_{11}$ melt-spun ribbons, with the aim to enhance their caloric properties and shift MT close to room temperature. It is found that the MT temperature decreases with the Cu addition, which is the opposite behavior to a well-known *e*/*a* rule.

However, it was experimentally confirmed that the unit cell volume effect is responsible for such a behavior. The substitution of Ni by Cu causes the unit cell volume to extend resulting in the decrease of the characteristic temperatures of MT. The crystal structure of alloys changes from two-phase structure where austenite is in grain interiors and martensite is located at the grain boundaries. Additionally, both the inverse magnetocaloric and elastocaloric effects in the vicinity of MT under moderate magnetic fields and stresses have been evaluated. Small addition of the fifth element, such as copper, strongly influences the structural and magneto-structural properties of the ribbons, also improving their functional properties important for applications.

Acknowledgements

The financial support of the Spanish Ministry of Economy and Competitiveness (project MAT2014-56116-C4-1-3-4-R) and Basque Government Department of Education (project IT711-13) is greatly acknowledged.

References:

[1] A. Ghosh, K. Mandal; J. Alloys Compd. 579 (2013) 295. DOI: 10.1016/j.jallcom.2013.06.062.

[2] D.Y. Cong, S. Roth, L. Schulz; Acta Mater. 60 (2012) 5335. DOI: 10.1016/j.actamat.2012.06.034.

[3] A. Ghosh, K. Mandal; Eur. Phys. J. B 86 (2013) 378. DOI: 10.1140/epjb/e2013-40489-0.

[4] T. Krenke, E. Duman, M. Acet, E.F. Wasserman, X. Moya, L. Mañosa, A. Planes; Nat. Mater. 4 (2005) 450. DOI: 10.1038/nmat1395.

[5] A. K. Pathak, I. Dubenko, C. Pueblo, S. Stadler, and N. Ali; J. Appl. Phys. 107 (2010) 09A907. DOI: 10.1063/1.3335893.

[6] D.Y. Cong, S. Roth, L. Schulz; Acta Matter. 60, 5335 (2012). DOI: 10.1016/j.actamat.2012.06.034.

[7] R. Das, S. Sarma, A. Perumal, A. Srinivastan; J. Appl. Phys. 109 (2011) 07A901. DOI: 10.1063/1.3540327.

[8] D.T. Huu, N.H. Yen, P.T. Thanh, N.T. Mai, T.D. Thank, T.-L. Phan, S. Ch. Yu, N. H. Dan; J. Alloys Compd. 622 (2015) 535. DOI: 10.1016/j.jallcom.2014.10.126.

[9] I. Dincer, E. Yüzüak, Y. Elerman; J. Alloys Compd. 506 (2010) 508. DOI: 10.1016/j.jallcom.2010.07.066.

[10] T.Krenke, M. Acet, E.F. Wassermann, X. Moya, Ll. Manosa, A. Planes; Phys. Rev. B 72 (2005) 14412. DOI: 10.1103/PhysRevB.72.014412.

[11] L. Pan-Pan, W. Jing-Min, J. Cheng-Bao; Chin. Phys. B 20 (2011) 028104. DOI: 10.1088/1674-1056/20/2/028104.

[12] J.M. Wang, C.B. Jiang; Scripta Mater. 62 (2010) 298. DOI: 10.1016/j.scriptamat.2009.11.023

[13] P.O. Castillo-Villa, L. Mañosa, D.E. Soto-Parra, J.L. Sánchez-Llamazares, H. Flores-Zúñiga, C. Frontera; J. Appl. Phys. 113 (2013) 053506. DOI: 10.1063/1.4790104.

[14] Z. Guo, L. Pan, M. Yasir Rafique, X. Zheng, H. Qiu, Z. Liu, J. Alloys Compd. 577(2012) 174. DOI:10.1016/j.jallcom.2013.04.102.

[15] B. Emre, N.M. Bruno, S.Y. Emre, I. Karaman, Appl. Phys. Lett. 105 (2014) 231910. DOI: 10.1063/1.4903494.

[16] F. Chen, Y.-X. Tong, B. Tian, L. Li, Y.-F. Zheng, Rare Met. 33 (2013) 516. DOI: 10.1007/s12598-013-0100-7.

[17] Y. Zhang, Q. Zheng, W. Xia, J. Zhang, J. Du and Y. A., Scripta Mater. 104 (2015) 41. DOI: 10.1016/j.scriptamat.2015.04.004.

[18] Z.D. Han, D.H. Wang, C.L. Zhang, H.C. Xuan, B.X. Gu, Y.W. Du; Appl. Phys Lett. 90 (2007) 042507. DOI: 10.1063/1.2435593

[19] B. Hernando, J.L. Sánchez Llamazares, J.D. Santos, Ll. Escoda, J.J. Suñol, R. Varga, D. Baldomir, D. Serantes, Appl. Phys. Lett. 92 (2008) 042504. DOI: 10.1063/1.2838356.

[20] J.L. Sánchez Llamazares, T. Sanchez, J.D. Santos, M.J. Pérez, M.L. Sanchez, B. Hernando Ll. Escoda, J. J. Suñol, R. Varga; Appl. Phys. Lett. 92 (2008) 012513. DOI: 10.1063/1.2827179.

[21] P. Czaja, W. Maziarz, J. Przewoźnik, A. Zywczak, P. Ozga, M. Bramowicz, S. Kulesza, J. Dutkiewicz; Intermetallics 55 (2014) 1. DOI: 10.1016/j.intermet.2014.07.001

[22] A. Wójcik, W. Maziarz, M. J. Szczerba, M. Sikora, J. Dutkiewicz, E. Cesari; Mater. Sci. Eng. B 209 (2016) 23. DOI: 10.1016/j.mseb.2016.03.002.

[23] J. D. Santos, T. Sanchez, P. Alvarez, M.L. Sanchez, J. L. S*á*nchez Llamazares, B. Hernando; J. Appl. Phys. 103 (2008) 07B326. DOI: 10. 1063/1.2832330.

[24] H. F. Tian, J. B. Lu, L. Ma, H. L. Shi, H. X. Yang, G. H. Wu, and J. Q. Li; J. Appl. Phys. 112 (2012) 033904. DOI: 10.1063/1.4740458.

[25] A. M. P*é*rez-Sierra, J. Pons, R. Santamarta, P. Vermaut, P. Ochin; Acta Mater. (2015). DOI: 10.1063/1.4740458.

[26] W. Maziarz, P. Czaja, J. Dutkiewicz, R. Wróblewski, M. Leonowicz, Mater. Sci.Forum 782 (2014) 23, DOI: 10.4028/www.scientific.net/MSF.782.23.

[27] W. Maziarz, P. Czaja, M.J. Szczerba, L. Lity´nska-Dobrzyńska, T. Czeppe, J.Dutkiewicz, J. Alloys Compd. 615 (2014) S173. DOI: 10.1016/j.jallcom.2013.12.164.

[28] H. Zheng, W. Wang, S. Xue, Q. Zhai, J. Frenzel, Z. Luo; Acta Mater. 61 (2013) 4648. DOI: 10.1016/j.actamat.2013.04.035.

[29] V.A. Chernenko; Scripta Mater. 40 (1999) 523. DOI: 10.1016/S1359-6462(98)00494-1.

[30] Z. Wu, Z. Liu, H. Yang, Y. Liu, G. Wu and R. C. Woodward; Intermetallics 19 (2011) 445. DOI: 10.1016/j.intermet.2010.10.010.

[31] W.J. Feng, L. Zuo, Y.B. Li, Y.D. Wang, M. Gao, G.L. Fang; Mater. Sci. Eng. B 176 (2011) 621. DOI: 10.1016/j.mseb.2011.02.003.

[32] K. R. Priolkar, D. N. Lobo, P. A. Bhobe, S. Emura and K. Nigam; EPL Europhys. Lett. 509 (2011) 38006.

[33] H. C. Xuan, P. D. Han, D. H. Wang and Y. W. Du; Intermetallics 54 (2014) 120. DOI: 10.1016/j.intermet.2014.05.022.

[34] L. H. Yang, H. Zhang, F. X. Hu, J. R. Sun, L. Q. Pan and B. G. Shen, J. Alloys Compd. 588 (2014) 46. DOI: 10.1016/j.jallcom.2013.10.196.

[35] M. Khan, J. Jung, S. S. Stoyko, A. Mar, A. Quetz, S. T., I. Dubenko, N. Ali, S. Stadler and K. H. Chow, Appl. Phys. Lett. 100 (2012) 172403. DOI: 10.1063/1.4705422.

[36] T. Kanomata, K. Shirakawa, T. Kaneko; J. Magn. Magn. Mater. 65 (1987) 76.

[37] C.O. Aguilar-Ortiz, D. Soto-Parra, P. Álvarez-Alonso, P. Lázpita, D. Salazar, P.O. Castillo-Villa, H. Flores-Zúñiga, V.A. Chernenko; Acta Mater. 107 (2016) 9. DOI: 10.1016/j.actamat.2016.01.041.

[38] J. M. Barandiaran, V. A. Chernenko, E. Cesari, D. Salas, P. Lazpita, J. Gutierrez, I. Orue; Appl. Phys. Lett. 102 (2013) 071904. DOI: 10.1063/1.4793412.

[39] V. Provenzano, A.J. Shapiro, R.D. Shull; Nature 429 (2004) 853. DOI: 10.1038/nature02657.

[40] F. Chen, Y. X. Tong, L. Li, J.L. Sánchez Llamazares, C.F. Sánchez-Valdés, P. Müllner; J. Alloys Compd. 691 (2017) 269. DOI: 10.1016/j.jallcom.2016.08.240.

[41] K.A. Gschneidner Jr, V.K. Pecharsky, A.O. Pecharsky, C.B. Zimm; Mater. Sci. Forum 315-317 (1999) 69.

[42] P. Álvarez-Alonso, C.O. Aguilar-Ortiz, E. Villa, A. Nespoli, H. Flores-Zúñiga, V.A. Chernenko; Scripta Mater. 128 (2017) 36. DOI: 10.1016/j.scriptamat.2016.09.033

[43] S.A. Nikitin, G. Myalikgulyev, M.P. Annaorazov, A.L. Tyurin, R.W. Myndyev, S.A. Akopyan, Phys. Lett. A 171 (1992) 234. DOI:

[44] F. Xiao, T. Fukuda, T. Kakeshita; Scripta Mater. 124 (2016) 133. DOI: 10.1016/j.scriptamat.2016.07.016.

Figure captions:

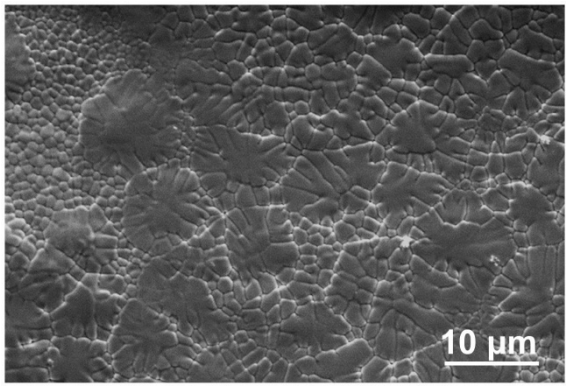

Figure 1. SEM SE micrograph taken from the free side for Cu1 ribbon.

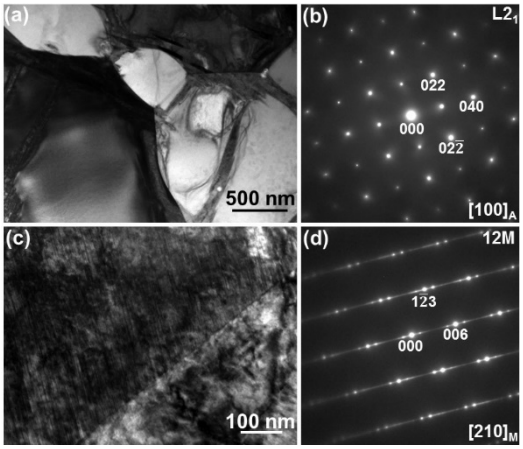

Figure 2. TEM BF image (a) and corresponding SAEDP (b) taken from the grain interior; TEM BF image (c) and SAEDP (d) taken from the grain boundary for Cu1 ribbon.

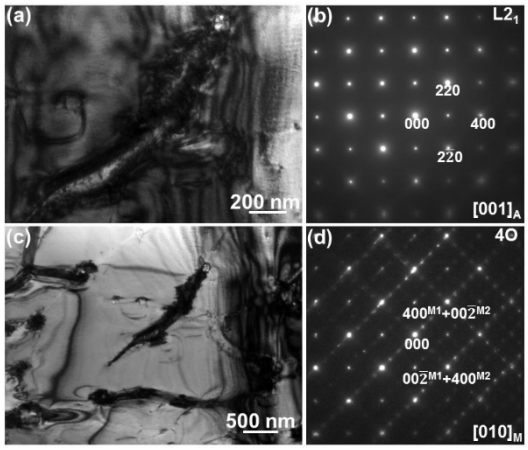

Figure 3. TEM BF images (a), (c) and corresponding SAEDPs (b), (d) for Cu3 ribbon.

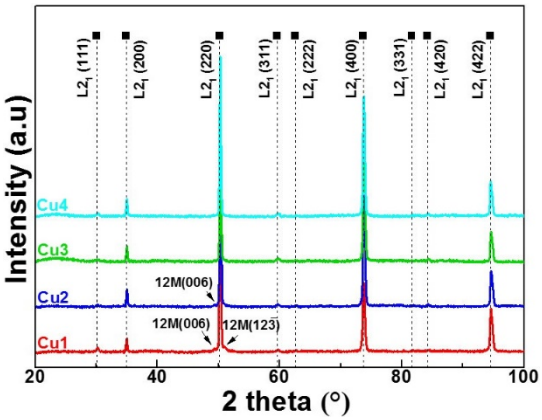

Figure 4. X-ray diffraction patterns of $Ni_{44-x}Cu_xCo_6Mn_{39}Sn_{11}$ (x=1, 2, 3, 4 at.%) measured at the free side of the ribbons at room temperature.

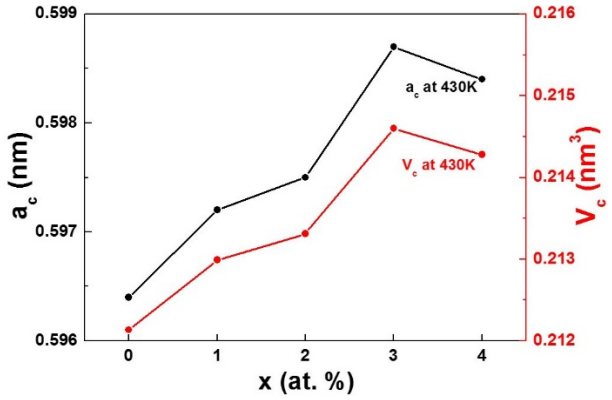

Figure 5. Dependence of lattice parameter a_c and unit cell volume V_c of paramagnetic austenite at temperature of 430 K on the concentration of Cu for all ribbons.

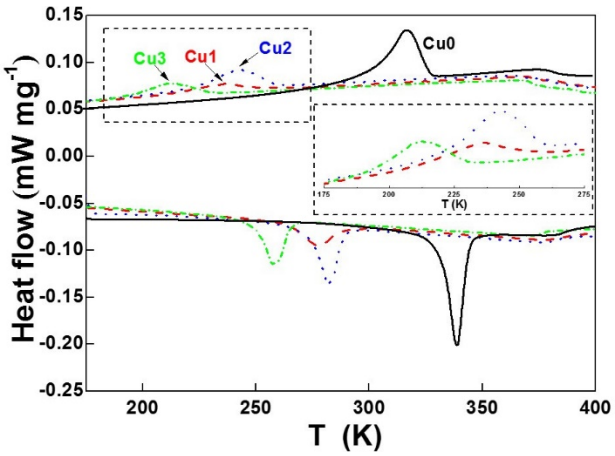

Figure 6. DSC curves for $Ni_{44-x}Cu_xCo_6Mn_{39}Sn_{11}$ (x=0, 1, 2, 3 at.) ribbons.

Please, remove Inset

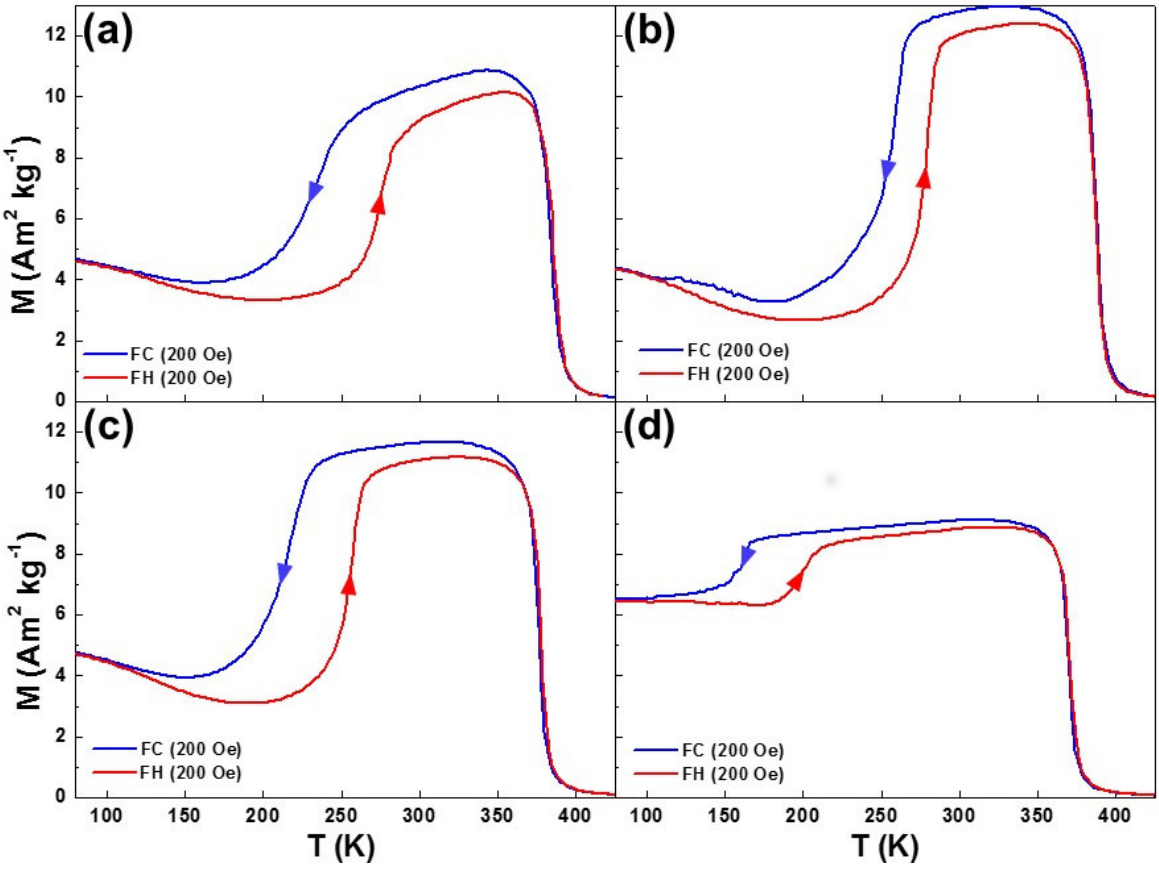

Figure 7. Thermomagnetization curves measured under magnetic field of 200 Oe for (a) Cu1, (b) Cu2, (c) Cu3, (d) Cu4 ribbons.

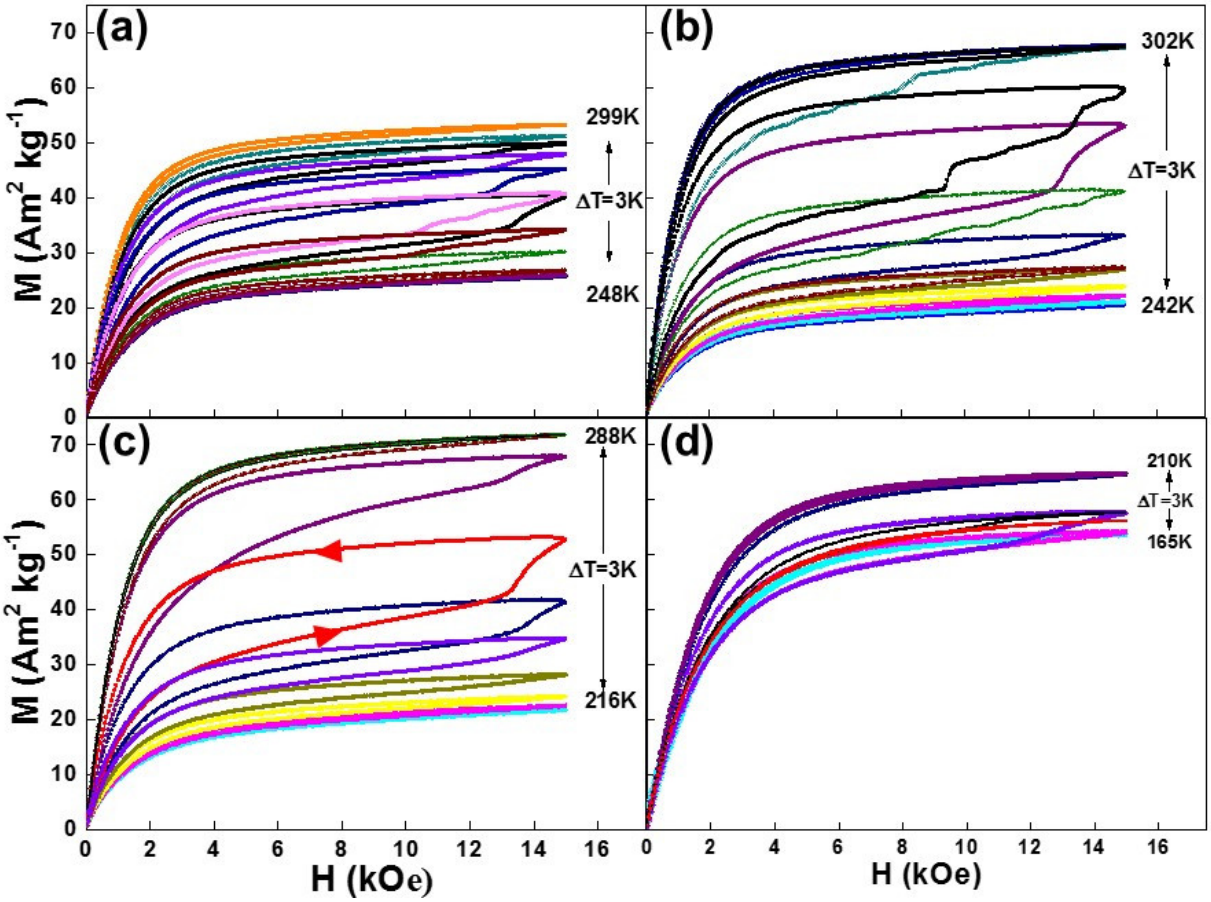

Figure 8. Magnetization curves measured at different temperatures in the vicinity of the martensitic transformation in the ribbons: (a) Cu1, (b) Cu2, (c) Cu3 and (d) Cu4.

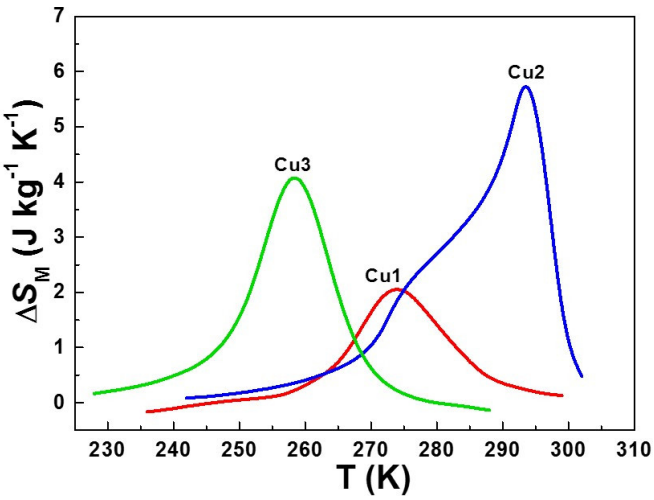

Figure 9. Temperature dependence of magnetic entropy change for Cu1, Cu2 and Cu3 ribbons in the magnetic field of 15 kOe.

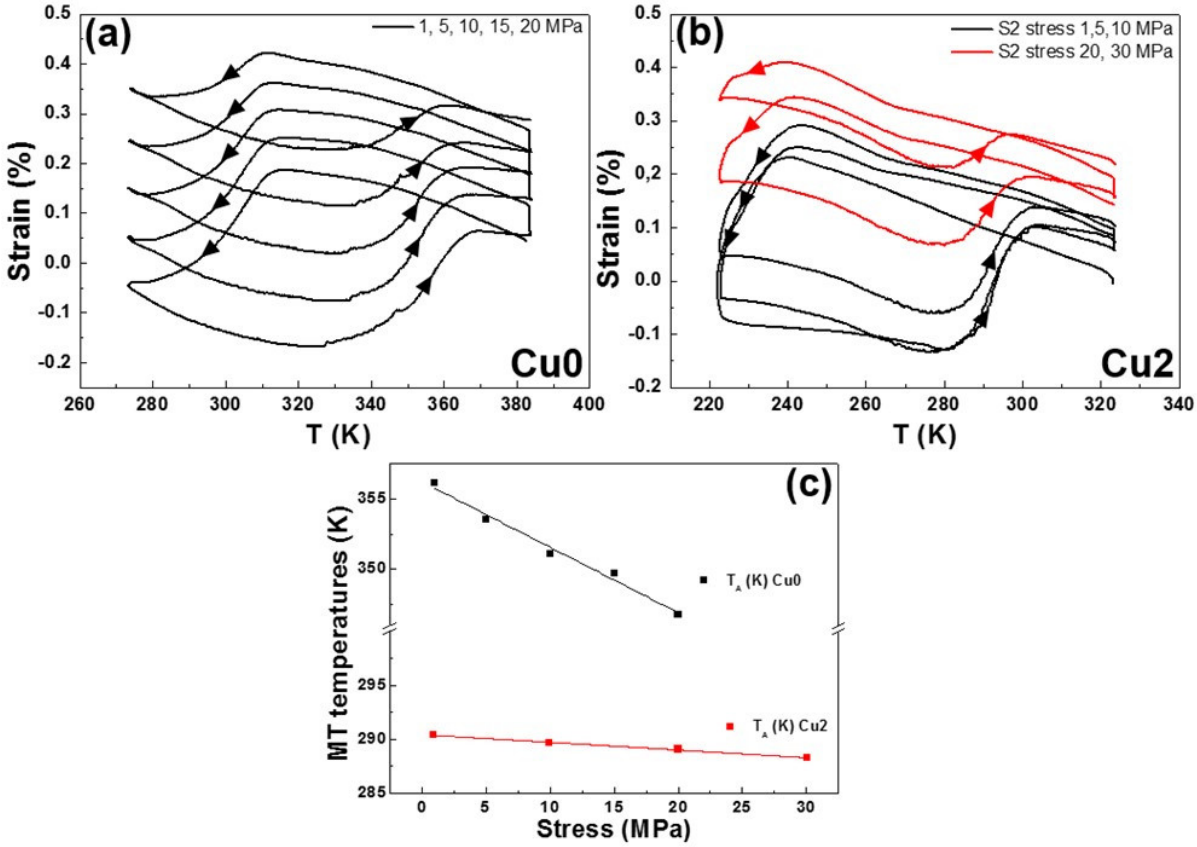

Figure 10. Temperature dependences of strain under various tensile stresses applied to Cu0 (a) and Cu2 (b) ribbons. Temperature of the reverse martensitic transformation, T_A, as a function of applied stress for the same ribbons.

Please, make curves on (a) and (b) in color. Think about how distinguish between them when they are published in black-and-white

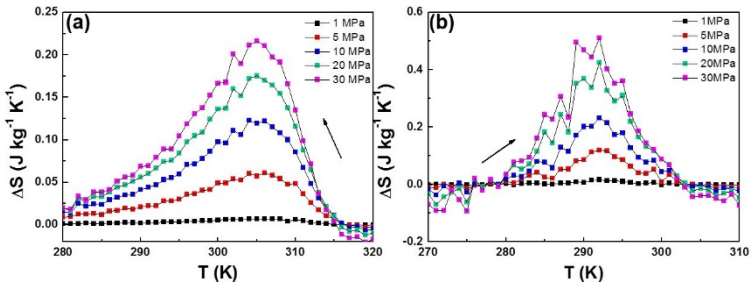

Figure 11. Temperature dependence of isothermal entropy changes for Cu0 upon cooling (a) and Cu2 upon heating (b).

Think about how distinguish between curves when they are published in black-and-white

Table 1. Actual chemical composition (in at.%) and electron concentration per atom (*e*/*a*) for $Ni_{44-x}Cu_xCo_6Mn_{39}Sn_{11}$ (x=1–4 at. %) ribbons.

Ribbon	Ni	Cu	Co	Mn	Sn	*e*/*a*
Cu1	42.4±0.3	1.3±0.1	6.1±0.1	39.6±0.1	10.6±0.1	8.13
Cu2	42.0±0.5	2.4±0.1	6.0±0.3	39.0±0.5	10.7±0.3	8.16
Cu3	41.0±0.4	3.3±0.1	6.2±0.1	38.7±0.3	10.7±0.3	8.16
Cu4	40.0±0.2	4.3±0.1	5.9±0.1	39.0±0.5	11.0±0.2	8.17

Table 2. Forward (T_M, T_{ms}, T_{mf}) and reverse (T_A, T_{as}, T_{af}) martensitic transformation temperatures, determined by DSC and magnetic measurements, thermal hysteresis (ΔT), Curie temperature of austenite (T_C^A), the averaged value of enthalpy for the forward and reverse MT ($|\Delta H|$) and the averaged entropy change at the transition ($|\Delta S|$) of $Ni_{44-x}Cu_xCo_6Mn_{39}Sn_{11}$ (x=0, 1, 2, 3, 4 at.%) ribbons.

Ribbon	Method	T_{ms} (K)	T_{mf} (K)	T_M (K)	T_{as} (K)	T_{af} (K)	T_A (K)	ΔT (K)	T_C^A (K)	$\|\Delta H\|$ (J g^{-1})	$\|\Delta S\|$ (J kg^{-1}K^{-1})
Cu0	DSC	329	301	315	332	345	339	16	-	9.3	27.7
	VSM	332	308	320	331	351	341	19	399	-	-
Cu1	DSC	251	209	230	263	284	274	33	-	2.2	8.2
	VSM	251	205	230	259	286	273	35	393	-	-
Cu2	DSC	260	209	235	281	292	287	32	-	3.8	13.8
	VSM	267	218	243	287	293	290	26	393	-	-
Cu3	DSC	230	192	211	236	267	252	37	-	3.3	13.3
	VSM	230	187	209	232	265	249	35	384	-	-
Cu4	DSC	-	-	-	187	208	198	-	-	-	-
	VSM	166	145	156	187	211	199	45	376	-	-